Efficient coupling into slow-light one-dimensional fishbone waveguide by mode converter method

2017 Appl. Phys. Express 10 072502

(http://iopscience.iop.org/1882-0786/10/7/072502)

Applied Physics Express **10**, 072502 (2017)
https://doi.org/**10.7567/APEX.10.072502**

Efficient coupling into slow-light one-dimensional fishbone waveguide by mode converter method

Xiangjie Zhao[1,2], Hamed Dalir[3]*, Xiaochuan Xu[3], and Ray T. Chen[2]*

[1]*Institute of Fluid Physics, China Academy of Engineering Physics, Mianyang 621900, China*
[2]*Department of Electrical and Computer Engineering, University of Texas at Austin, Austin, TX 78758, U.S.A.*
[3]*Omega Optics Inc., Austin, TX 78759, U.S.A.*

*E-mail: hamed.dalir@omegaoptics.com; chenrt@austin.utexas.edu

Received March 15, 2017; accepted May 31, 2017; published online June 14, 2017

The high-order mode in a fishbone waveguide accommodates the easy manipulation of group index dispersion. To minimize Fresnel reflection, group velocity mismatch can be compensated for by a casual step taper, but with low coupling efficiency. Here, we propose a mode converter to boost the coupling efficiency to in and out of the slow-light fishbone waveguide. Split, phase, and side slots in a mode converter are employed to compensate for the mode mismatch in terms of the width of the lobes, the phase offset, and the power ratio between neighboring lobes. A high coupling efficiency of ~70% leads to the efficient compact true-time delay required for phased array antennas.

The slow-light waveguide has been studied for various areas such as nonlinear optics, optical buffers, true time delay (TTD), high-speed devices, and optical amplifiers.[1–4] Among them, the slow-light photonics crystal waveguide (PCW) has been attracting much attention because of its ultracompact footprint; however, its fabrication process is still a key issue.[5–7] The one-dimensional (1D) silicon fishbone waveguide possesses a reasonable scattering loss and is easily fabricated at a low cost.[8,9] However, the engineering implementation of the 1D silicon fishbone waveguide is limited by the inadequate dispersion of the group index and the low coupling efficiency of light in and out of the 1D silicon fishbone waveguide.[10–14] Note that the slow light in the 1D silicon fishbone waveguide can be designed at the band edge, while the curvature of the band edge will determine the group index dispersion.[15] To realize a large group dispersion increase, mode overlap with the fishbone structure is indispensable. To this end, a higher band with a higher-order mode would be preferred to enlarge the group index dispersion with a reasonable optical loss.[7,11] In contrast, owing to the poor slow-light coupling performance, such a higher band in the fishbone waveguide is rarely employed in practical applications.

The most common ways of coupling the slow light into a PCW are evanescent field generation and anti-Fresnel reflection.[16–19] Evanescent field generation is mostly studied in the two-dimensional (2D) or three-dimensional (3D) PCW, while a grating layered structure along the propagation direction is required. In the case of the 1D silicon fishbone waveguide, no grating layered structure can support the evanescent field generation. Thus, the anti-Fresnel reflection method such as the use of an adiabatic or step taper is employed to improve the slow-light coupling performance.[11,19,20] However, the adiabatic taper does not support the slow-light coupling to a higher-band fishbone waveguide owing to the existence of a band gap that is just below the desired band. Note that the anti-Fresnel reflection method such as the use of a step taper would compensate for the group velocity mismatch and hence reduce the reflection loss. However, in many higher bands with a large flexibility of the group index dispersion, mode mismatch is significant. The existing higher-order mode usually spreads across the backbone and teeth regions, with multiple lobes and π radian phase offset between neighboring regions. Thus, mode mismatch would be very large and thus cannot be considered in the slow-light coupling except for group velocity matching.[21]

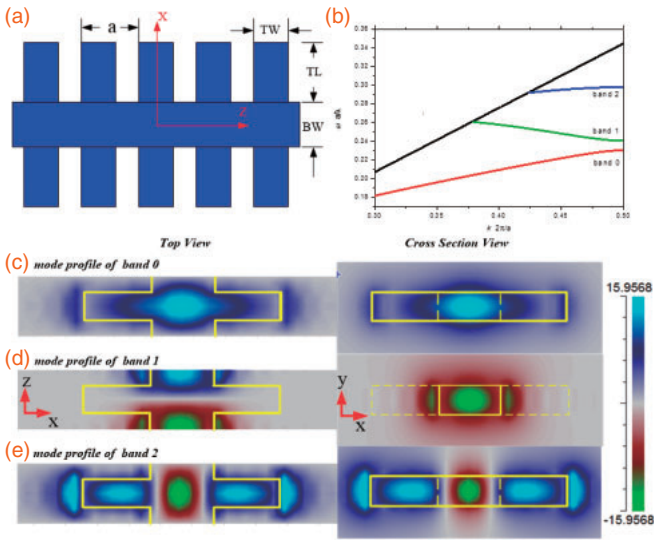

Fig. 1. (a) Structure of the fishbone waveguide, specified by teeth width (TW), teeth length (TL), backbone width (BW), and teeth period. (b) Band diagram of the fishbone waveguide when $TL = 500$ nm, $a = 450$ nm, and $TW = 0.45a$. The top and cross-sectional views of the electric-field mode profiles of bands 0, 1, and 2 are given in (c), (d), and (e), respectively.

In this study, the mode mismatch effect on the slow-light coupling is first elucidated. A new slow-light coupler method based on a mode converter is then proposed to couple slow light into band 2 of the fishbone waveguide. Both mode and group velocity mismatches between strip and fishbone waveguides are compensated for by employing this novel coupler. Numerical simulation is performed to realize a high coupling efficiency of 70% for band 2. This device concept is crucial for next-generation beam steering devices as well as high-speed computing systems.

The structure of the fishbone waveguide is shown in Fig. 1(a). The fishbone waveguide consists of a backbone region and a periodic teeth region on both sides of the backbone along the z-direction. The structure of the fishbone waveguide is specified by teeth width (TW), teeth length (TL), backbone width (BW), and teeth period (a). Figure 1(b) depicts the band diagram of the fishbone waveguide, with $TL = 500$ nm,

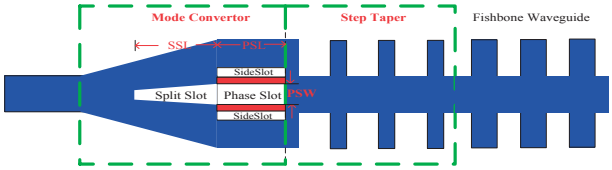

Fig. 2. Schematic of the proposed coupler based on mode converter method. The split slot length (SSL), phase slot length (PSL), and phase slot width (PSW) are specified here as 4.5a, 4.5a and 310 nm, respectively. The length of the mode converter is fixed at 8.5a. A larger mode converter length will lead to better coupling.

$a = 450$ nm, and $TW = 0.45a$. The top and cross-sectional views of the mode profiles of bands 0, 1, and 2 are given in Figs. 1(c)–1(e), respectively. According to the fabrication procedure of the silicon fishbone waveguide, the width of the backbone is usually around 450–500 nm. This will minimize the propagation loss due to the tough surface of the backbone sidewall. By exhaustively scanning the structure parameters, not only will the dispersion of the group index be increased but also the desired higher band edge can be controlled and optimized. By considering the actual silicon-on-insulator (SOI) material and propagation loss, the BW and height of the fishbone are fixed at 450 and 220 nm, respectively. According to the scaling law of photonic crystals, the band edges of the two bands are both normalized to be around 1532 nm.

The major electric field component (E_x) in one period unit is calculated for bands 0, 1, and 2 by a 3D plane wave expansion method. It is indicated that both the mode profiles of bands 0 and 1 behave like a fundamental mode and are similar to the strip waveguide. Namely, the electric field mode matching between the strip and fishbone waveguides for bands 0 and 1 is good. In this case, mode mismatch is negligible and the anti-Fresnel reflection method would work well to reduce the Fresnel reflection loss. In the case of band 2, the electric field mode profile shown in Fig. 1(e) spreads across the teeth and backbone regions, with three lobes and π radian phase offset between neighboring lobes. The two side lobes mainly concentrate in the teeth region and are symmetrical with each other relative to the z-axis. The band 2 mode profile behaves like a higher-order transverse mode, so that the mode mismatch between the fundamental strip waveguide and the band 2 fishbone waveguide would become significant. The significant mode mismatch will attenuate the coupling to the slow-light region.[22)]

As shown in Fig. 2, a novel coupler to realize a high coupling efficiency to a fishbone waveguide is proposed. Here, the mode converter converts the fundamental mode of the strip waveguide to the higher-order mode of the fishbone waveguide, leading to a reduction in mode mismatch. Besides, a step taper is cascaded to further suppress the Fresnel reflection.

The strip waveguide is expanded to match with the fishbone width. A split slot is positioned in the middle of the fishbone waveguide along the z-direction. Owing to the fabrication limitation, the split slot width is 120 nm. Note that the partial energy of the incident light will be coupled into the split slot, while the rest will propagate along both sides of the split slot, leading to the generation of three lobes. The phase slot follows the split slot to tune the actual phase offset between the central lobe and the neighboring side lobes. The

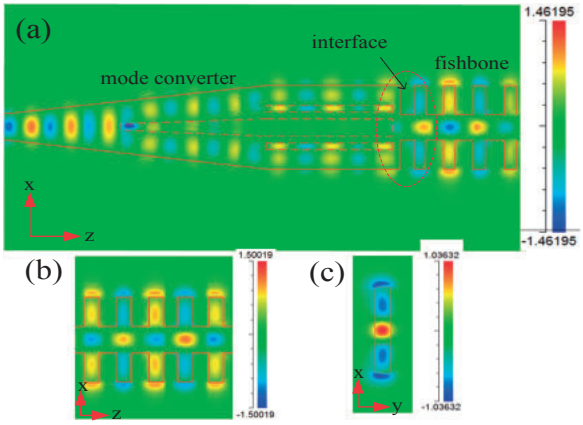

Fig. 3. (a) Electric field (E_x) of the incident light passing through the mode converter without a step taper. (b) Top and (c) cross-sectional views of the major electric field mode profile of band 2 along the propagation direction. The results were calculated by the 3D FDTD method.

phase slot width is the same as the ending point of the split slot. Two side slots are introduced to support the separation of the three lobes. The ending point of the phase slot is a half teeth width in length away from the curved teeth edge of the 1D fishbone waveguide, as illustrated in Fig. 2. After passing through the mode converter, the converted mode becomes similar to the band 2 mode profile shown in Fig. 1(e). Considering the fabrication restriction, the widths of the side slots and red silicon strip are set to be 120 and 110 nm, respectively. It should be pointed out that the coupler shown in Fig. 2 is on the in-port of the fishbone, while the coupler on the out-port of the fishbone is not shown here.

The major electric field (E_x) component of the incident light passing through the mode converter without a step taper is recorded by 3D finite-difference time-domain (FDTD) numerical simulation, which is shown in Fig. 3(a) and expanded into the fishbone region. With the help of the mode converter coupling, the band 2 mode profile of the fishbone waveguide is also recorded by the 3D FDTD method and depicted in Figs. 3(b) and 3(c). The recorded electric field mode profiles shown in Figs. 3(b) and 3(c) are the same as the mode profile shown in Fig. 1(e). As indicated in Fig. 3(a), the input light from the conventional strip waveguide is first divided into three lobes by the split slot. Then, the phase offset between neighboring lobes is tuned by the phase slot. It is shown at the interface region that the mode mismatch between the strip waveguide and the fishbone waveguide is significantly compensated for after the light passes through the mode converter.

Here, we compared our novel coupler performance with respect to butt and step taper coupling by exploiting numerical simulation using the FDTD method. As for the butt coupling case, the strip waveguide was connected to the fishbone waveguide directly without using any coupler. The coupling performance is shown in Fig. 4(a). Both butt and step taper coupling cases without a mode converter will provide an efficient slow-light coupling into bands 0 and 1. The band edge locations of bands 0 and 1 are consistent with that calculated from the band diagram shown in Fig. 1(b). However, no light is found to be coupled into band 2, whose band edge should be located at around 1538 nm. Only coupling to the radiation mode is found there. To further prove the inefficient slow-light coupling performance by using a step taper, the

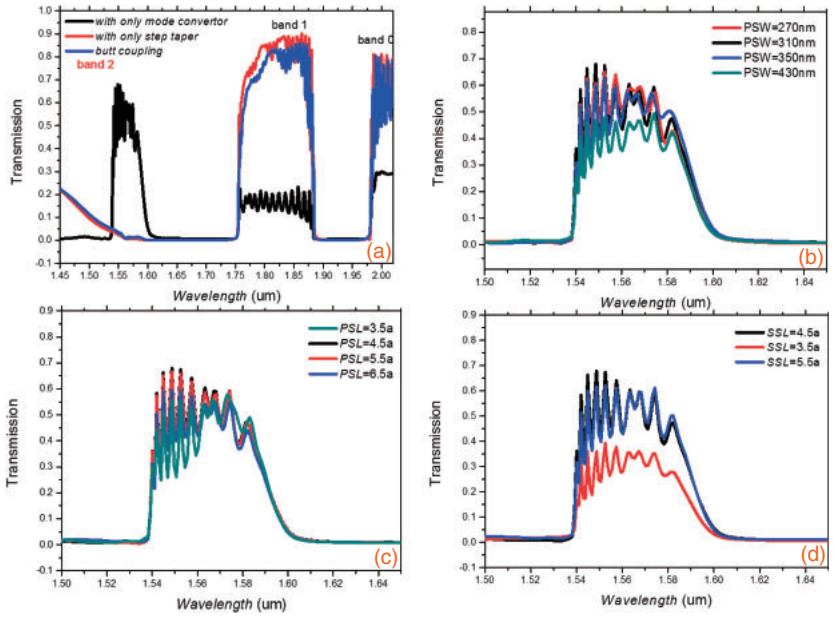

Fig. 4. (a) Slow-light coupling comparison for bands 0, 1, and 2 using butt, step taper, and mode converter coupling. For the step taper coupling, the taper teeth length, taper teeth width, and taper teeth period are fully scanned to optimize the coupling performance. (b) Slow-light coupling performance of mode converter method by scanning phase slot width (PSW). (c) Slow-light coupling performance of mode converter method by scanning phase slot length (PSL). (d) Slow-light coupling performance of mode converter method by scanning split slot length (SSL).

taper teeth length, taper teeth period, and taper teeth width are fully scanned to check the band 2 slow-light coupling performance. The optimized parameters indicate that light cannot be coupled into band 2 using a step taper. (The significant mode mismatch blocks light from coupling into band 2.)

In contrast, efficient slow-light coupling performance into band 2 is found by the mode converter method, as shown in Fig. 4(a). The average transmission efficiency exceeded 55% and the maximum coupling efficiency could be as high as 70%. Compared with the 0% coupling efficiency based on the step taper and butt coupling methods, the coupling efficiency significantly increased. The radiation mode is also found to disappear, which also partly increases the efficiency of coupling into the slow-light region. Note that the proposed mode converter cannot fully convert energy from the fundamental mode into another mode. For instance, the remaining energy coupling into bands 0 and 1 after passing through the mode converter is about 20%, which cannot be coupled into band 2. To optimize the mode converter structure, all parameters are carefully designed to compensate for the mode mismatch. The numerical results are shown in Figs. 4(b)–4(d). The phase slot width determines the central lobe width after passing through the mode converter. As shown in Fig. 4(b), the optimized phase slot width is 310 nm, which is much smaller than the backbone width. The phase slot length will mainly determine the phase offset between neighboring lobes. As plotted in Fig. 4(c), the coupling performance would be maximized when the phase slot length is $4.5a$ (the desired phase offset between neighboring lobes should be absolutely π radians). In the case of large-bandwidth coupling, there will be a tradeoff between the bandwidth and the monochromatical phase offset. The split slot length will determine the actual power ratio between neighboring lobes. As illustrated in Fig. 4(d), the optimized split slot length should be $4.5a$.

Although the coupling efficiency could be increased from 0% to as high as 70% by compensating for the mode mismatch using the mode converter, observable Fabry–Pérot (FP) oscillation patterns are still seen in Fig. 4. For real engineering application, two couplers would be needed on the in- and out-ports of the fishbone waveguide, which construct the FP cavity in numerical simulation. The oscillation patterns mainly originate from the Fresnel reflection and group velocity mismatch between the mode converter and the fishbone waveguide. With increasing fishbone length, the oscillation cycle would be reduced to be dense. In view of the anti-Fresnel reflection method, the step taper can be inserted between the mode converter and the fishbone waveguide to eliminate these oscillation patterns. As for step taper definition, teeth width or teeth length can be tapered to form the step taper, which functions to reduce the group velocity mismatch. As shown in Fig. 5(a), the band diagram would be lifted up by the taper teeth width (step taper 1) or teeth length (step taper 2). The lifted band diagram can be employed to construct the step taper, which will be inserted between the mode converter and the fishbone waveguide. The constructed step taper compensates for the group velocity mismatch and reduces the Fresnel reflection loss. The mode profile obtained by scanning the teeth length and width is shown in Fig. 5(b). We figured out that the mode match would be well maintained by tapering the teeth width, while teeth length tapering should be avoided.

In the final design of the step taper, the taper teeth width is reduced from $0.45a$ to $0.415a$, while the taper teeth length remains unchanged [step taper 1 in Fig. 6(a)]. This maintains the mode matching condition between the mode converter and the fishbone waveguide. It is shown that the FP oscillation patterns are clearly eliminated near the band edge of band 2. The transmission of slow-light coupling into band 2 at 1543 nm can be increased from about 37 to 70%. Coupling transmission using the step taper with reduced teeth length [step taper 2 in Fig. 6(a)] is also compared here. It is clear that oscillation patterns are not improved, because the mode matching condition is destroyed by the insertion of step

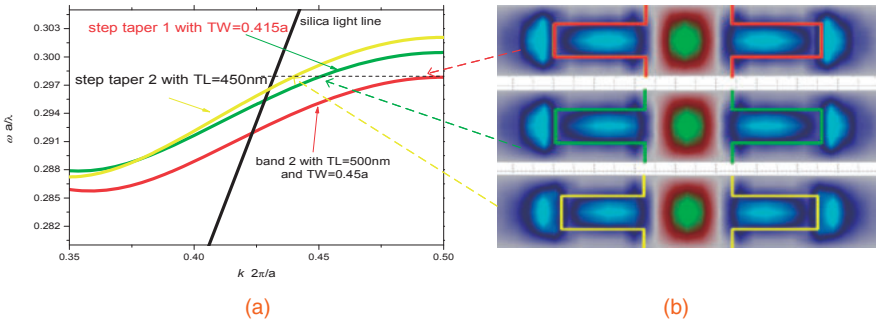

Fig. 5. Band diagram of the inserted step taper shown in Fig. 2 with taper teeth width (*TW*) (step taper 1) or length (*TL*) (step taper 2), in comparison with the band 2 diagram of the fishbone waveguide. The right side indicates the mode profile of these three band diagrams at $\omega = 0.297$.

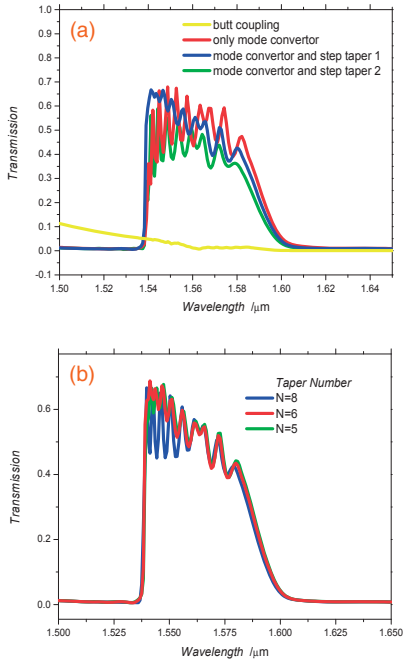

Fig. 6. (a) Coupling efficiency of proposed coupler by cascading a step taper after a mode converter, in comparison with that of the mode converter and butt coupling methods. The inserted step tapers 1 and 2 are specified in (b), where slow-light coupling performance obtained by varying the step taper period number *N* is also shown.

taper 2. In fact, the insertion of any optimized step taper cannot guarantee a perfect mode matching condition, which would probably contribute to the reduction in coupling efficiency. Fortunately, the slow-light region is mainly located between the band edge and 1560 nm. The proposed hybrid coupler by cascading the mode converter and step taper behaves differently from the pure step taper coupler. As shown in Fig. 6(b), the coupling efficiency would decrease when the step taper length deviates from six periods. Although the group velocity mismatch can be compensated for by increasing the cascaded step taper length, it would also contribute to the generation of mode mismatch.

In conclusion, a novel slow-light coupler based on a mode converter is proposed for the band 2 fishbone waveguide. Mode and group velocity mismatches are well compensated for simultaneously. In the design of the mode converter, split and phase slots are employed to generate multiple lobes and tune the phase offset between neighboring lobes. After passing through the mode converter, the strip fundamental mode can be converted into the desired higher-order mode of band 2. The group velocity mismatch will also be compensated for by cascading the step taper after the mode converter, which helps to reduce the Fresnel reflection and eliminate the interference oscillation patterns of transmission spectra. The numerical simulation by the 3D FDTD method indicates that the transmission for slow-light coupling into band 2 can be enhanced from 0% to as high as 70%. This novel coupler can be extended to couple slow light into other higher bands crucial for phase array antennas.

Acknowledgments This work was supported by the National Natural Science Foundation of China (Grant Nos. 61378095 and 61575179) and Air Force Office of Scientific Research (AFOSR) Small Business Innovation Research (SBIR) program under award number FA9550-16-C-0033.

1) C. Y. Lin, H. Subbaramane, A. Hosseini, A. X. Wang, and L. Zhu, Appl. Phys. Lett. **101**, 051101 (2012).
2) R. J. P. Engelen, Y. Sugimoto, Y. Watanabe, J. P. Korterik, N. Ikeda, N. V. van Hulst, K. Asakawa, and L. Kuipers, Opt. Express **14**, 1658 (2006).
3) Y. A. Vlasov, M. O'Boyle, H. F. Hamann, and S. J. McNab, Nature **438**, 65 (2005).
4) J. Garcia, P. Sanchis, A. Martinez, and J. Marti, Opt. Express **16**, 3146 (2008).
5) Y. Hamachi, S. Kubo, and T. Baba, Opt. Lett. **34**, 1072 (2009).
6) A. Hosseini, X. C. Xu, D. N. Kwong, H. Subbaraman, W. Jiang, and R. T. Chen, Appl. Phys. Lett. **98**, 031107 (2011).
7) A. Brimont, J. V. Galan, J. M. Escalante, J. Marti, and P. Sanchis, Opt. Lett. **35**, 2708 (2010).
8) S. Hughes, L. Ramunno, J. F. Young, and J. E. Sipe, Phys. Rev. Lett. **94**, 033903 (2005).
9) H. Yan, X. C. Xu, C. J. Chung, H. Subbaraman, Z. Y. Pan, S. Chakravarty, and R. T. Chen, Opt. Lett. **41**, 5466 (2016).
10) A. Y. Petrov and M. Eich, Appl. Phys. Lett. **85**, 4866 (2004).
11) C. Bao, J. Hou, H. Wu, E. Cassan, L. Chen, D. Gao, and X. Zhang, IEEE Photonics Technol. Lett. **24**, 7 (2012).
12) C. M. Sterke, J. Walker, K. B. Dossou, and L. C. Botten, Opt. Express **15**, 10984 (2007).
13) P. Pottier, M. Gnan, and R. M. D. L. Rue, Opt. Express **15**, 6569 (2007).
14) D. Gao, J. Hou, R. Hao, H. Wu, J. Guo, E. Cassan, and X. Zhang, IEEE Photonics Technol. Lett. **22**, 1135 (2010).
15) M. L. Povinelli, S. G. Johnson, and J. D. Joannopoulos, Opt. Express **13**, 7145 (2005).
16) C. Y. Lin, X. Wang, S. Chakravarty, W. C. Lai, B. S. Lee, and R. T. Chen, Proc. SPIE **7944**, 79440K (2011).
17) A. Oskooi, A. Mutapcic, S. Noda, J. D. Joannopoulos, S. P. Boyd, and S. G. Johnson, Opt. Express **20**, 21558 (2012).
18) C. Y. Lin, X. Wang, S. Chakravarty, B. S. Lee, W. C. Lai, and R. T. Chen, Appl. Phys. Lett. **97**, 183302 (2010).
19) C. M. de Sterke, K. B. Dossou, T. P. White, L. C. Botten, and R. C. McPhedran, Opt. Express **17**, 17338 (2009).
20) F. J. Lawrence, Dissertation of The University of Sydney, Sydney, Australia (2012).
21) M. F. Lu and Y. T. Huang, Jpn. J. Appl. Phys. **47**, 1822 (2008).
22) Z. Pan, H. Subbaraman, Y. Zou, X. Xu, X. Zhang, C. Zhang, Q. Li, L. J. Guo, and R. T. Chen, Photonics Res. **3**, 317 (2015).